POAC'17
Busan, KOREA

Proceedings of the 24th International Conference on
Port and Ocean Engineering under Arctic Conditions
June 11-16, 2017, Busan, Korea

Thermodynamic Consolidation of Ice Rubble in the Small Scale in-situ Experiment. Van Mijen Fiord, Spitsbergen, March 2016

Aleksey Shestov[1], Evgenii Salganik[2]
[1] The University Centre in Svalbard, Longyearbyen, Norway
[2] Sustainable Arctic Marine and Coastal Technology (SAMCoT), Centre for Research-based Innovations (CRI), Norwegian University of Science and Technology, Trondheim, Norway

ABSTRACT

In March 2016 ice rubble thermodynamic consolidation experiment was performed in saline Lake Vallunden connected through a narrow straight to Van Mijen Fiord, Spitsbergen. Ice blocks of 23 x 23 x 5 cm were produced from the level ice section 1 x 1 x 0.6 m and placed back into the appeared basin. Ice rubble field was equipped with thermistor string probe through it and three one-point measurement conductivity and temperature sensors. Two of them were placed inside cavities between ice blocks in the upper and lower parts of the rubble, and the third one was located in sea water below the rubble. Part of the main phase of ice rubble thermodynamic consolidation due to atmospheric cooling was observed during 14 days. The developing of the consolidated layer and salt balance processes inside rubble cavities were observed and measured. Water inside cavities was found to be supercooled up to 0.3 °C. The final thickness of the consolidated layer, as defined by isoline corresponding to sea water freezing temperature and zero temperature gradient, by mechanical drilling and by Stefan's equation, was found to be 23, 30 and 29 cm correspondingly.

KEY WORDS: Ice Rubble, Thermodynamics, Consolidation, In-situ Experiment

INTRODUCTION

Arctic ice cover is rapidly changing, and it is most obviously seen in the summer ice extent. Ice is losing in thickness too. For example, Renner et al. (2014) report thinning by over 50% during 2003-2012. Such changes affect dynamic and thermodynamic models of ice cover – ocean interaction. Ice cover becomes more fragile and exposed to air and ocean interactions. The rate of deformation and speed of drift are increasing (Spreen et al., 2011). Ice ridges constitute a significant part of the ice volume (see e.g. Hansen et al. (2013)). As more of the Arctic sea ice becomes first-year, a larger fraction of the total volume will be first-year ridges. An essential difference between first-year and old ridges is that the former melt more easily, so the Arctic ice cover as a whole becomes more sensitive to global warming. Ice ridges are key feature both in geophysical context and in the engineering context. They often give the quasi-static design forces on marine structures when icebergs are not a threat (CAN/CSA-S471-92, R2001; ISO/FDIS/19906, 2010; SNiP2.01.07-85, 1987).

The role of ice ridges in the global heat and mass balance has not been studied extensively, and in particularly their role in a thinning Arctic sea ice cover needs to be better quantified. Strub-Klein and Sudom (2012) and Timco and Burden (1997) give comprehensive literature reviews of ridge studies from 1976 and onwards in the engineering context. Very few of the

ridge studies investigated the seasonal development of ridges, exceptions are, to the authors' knowledge, Leppäranta et al. (1995), Blanchet (1998), Høyland (2002) and Strub-Klein and Høyland (2011). Thermodynamic processes in ice ridges define their morphology structure and, as a result, mechanical properties too. These properties are essential for estimating ridge loads. The three last papers mostly deal with the consolidated layer, whereas the campaign of Leppäranta et al. (1995) measured the season development of the consolidated layer, temperature profiles, the keel depth and volume and the ridge and rubble macro-porosities and extended into the decay phase. Shestov and Ervik (2016) report on ice ridges studies in the Arctic Ocean during at the end of the main phase and the beginning of the decay phase.

Usually, the life cycle of first-year ice ridges from their formation to break up is divided into three phases: initial, main and decay. In case first-year ice ridge survives the summer and its decay phase, it becomes a second-year ice ridge. The initial phase is relatively short and characterized by formation and thermodynamic processes mostly related to extraction of reserved cold from submerged ice blocks, though oceanic heat flux and atmospheric cooling are present at the same time. The main phase is related to atmospheric cooling, and it is the phase when most of the consolidated layer growth occurs. The decay phase starts when ridge begin to be heated both from the ocean and the atmosphere. Summer transformation processes of ice ridges during the decay phase are not well understood yet but include both mechanical erosion and thermal effects. Shestov and Marchenko (2016b) and Shestov and Marchenko (2016a) considered thermodynamics of ice rubble in the water with the varying freezing point, due to freshening during the decay phase and showed that it could cause further consolidation (reduction of macro-porosity) to the keel. The presence of the brine pockets in the sea ice and the conditions of thermodynamic equilibrium explain a strongly non-linear specific heat capacity of sea ice. In the conditions of water freshening, this results in transferring energy from brine pockets to rubble cavities and reduction in macro-porosity of rubble due to an increase of its micro-porosity.

In both aspects, geophysics and engineering, ice ridges are the ice features of the interest for studying. Authors are involved in laboratory size, small field size and full-scale size studies and consider also performing basin and mesoscale size studies. This paper is dedicated to the small-scale field studies performed during March 2016 in Van Mijen Fjord, Spitsbergen. Due to seasonal ice conditions, the location of the experiment was chosen at the Lake Vallunden, connected with the fiord through a strait. Thus, the lake is filled with salt water and covered by saline ice. Ice rubble field was produced in a basin of 1 by 1 m and temperature and conductivity measurements in the rubble were organized. The aim was put on tracking initial phase and development of the consolidated layer both through the change in temperature pattern and salinity in rubble cavities.

EXPERIMENTAL SETUP AND METHODS

The setup and preparation stages are illustrated in Figure 1. Chainsaw operation was involved in opening up the basin and producing ice blocks. First, four large ice cubes were lifted up and left in the air overnight to accumulate more reserved cold. Next day 188 ice blocks of average dimensions 23 cm x 23 cm x 5 cm were prepared from large ice cubes. To avoid contacts between ice blocks and basin walls rope net was set inside the basin. This simplified lifting of the rubbles at the end of the experiment. Ice blocks were one by one placed into the basin and sensors were deployed in parallel. Thermistor string (TSP) probe was deployed through the rubble field, and three conductivity and temperature sensors (CTS) were

deployed: two inside the rubble (CTS1 and CTS2) and one under rubble (CTS3). Development of the rubble and its consolidated layer was monitored in such setup during two weeks from the beginning of March. At the end of the experiment newly frozen ice was cut through along the walls of the basin and consolidated ice rubble was lifted up in the net using engine crane with the help of a snowmobile. Once it was lifted, it was observed, pictured, sensors were recovered and samples were cored through the consolidated layer.

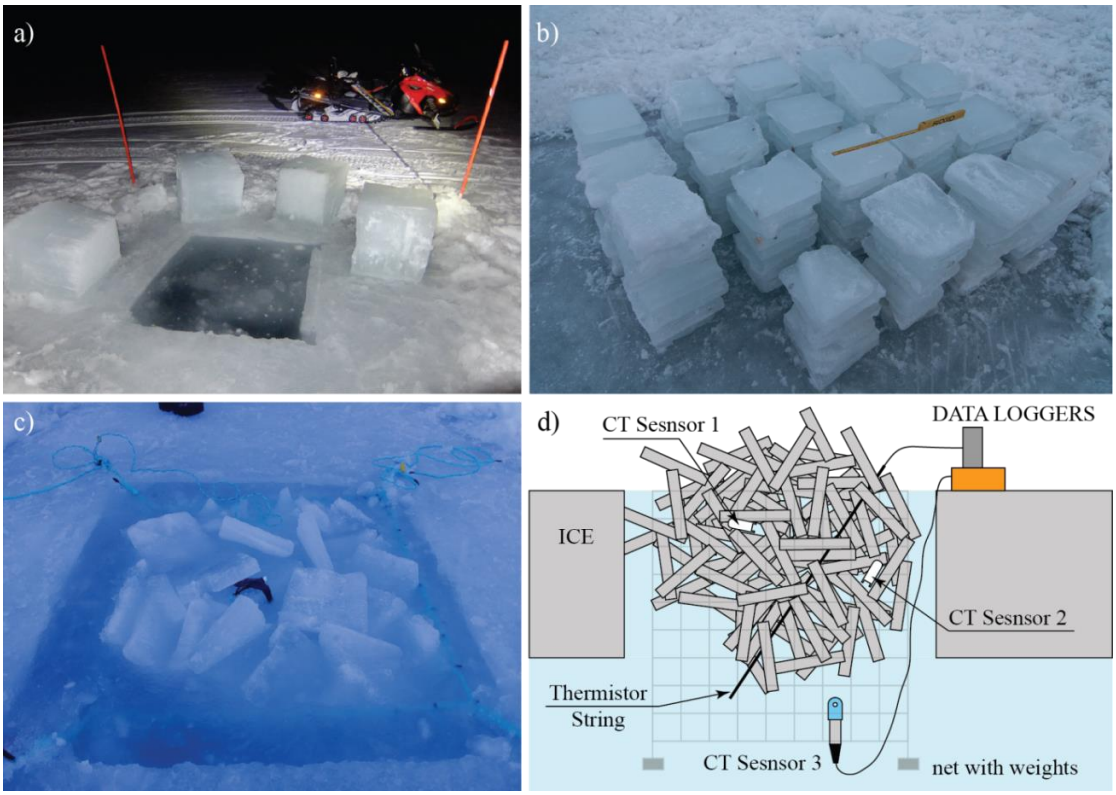

Figure 1. Experimental setup. Production of the basin and ice for rubble blocks (a). Prepared ice rubble blocks (b). The process of submerging ice rubble blocks into the basin and deployed CTS2 sensor (c). Schematic view of the whole experimental setup.

CTS1 and CTS2 sensors are autonomous sensors DST CT Type I (3-37 mS/cm) conductivity and temperature loggers (Star-Oddi, 2017). CTS3 is the Aanderaa conductivity/temperature sensor 4120 with analog output and external data logger. CTS1 and CTS2 provide conductivity measurements transferred in practical salinity units PSU. CTS3 provide conductivity measurements in mS/cm. Using a corresponding sequence of function from the TEOS-10, all salinities further are reported on the TEOS-10 absolute scale, S_a, (IOC et al., 2010) with salinity anomaly taken from version 3.0 of the McDougall et al. (2012) database. Conservative temperature freezing point is found using the corresponding function of TEOS-10 (IOC et al., 2010). TSP is the thermistor string from GeoPrecision GmbH company (GeoPrecision, 2017) with a sequence of measuring points spaced 4 cm apart from each other and external data logger. Readings from TSP were used to calculate vertical conductive heat flux according to Fourier's law, where temperature gradient was calculated between each two sequent TSP measuring points and the thermal conductivity was chosen to be 2.1 $Wm^{-1}K^{-1}$. Based on physical properties of sea ice measured in situ and using the model of thermal conductivity proposed by Schwerdtfeger (1963), Shestov et al. (2017) found the coefficient of thermal conductivity to be varying through the depth of ridge keel from 2.0 to 2.2 $Wm^{-1}K^{-1}$. Thus average value was chosen to be used in current estimates of conductive heat flux through the rubble.

RESULTS

During the experiment, there were two major atmospheric cooling events (Figure 2a). Though at the very beginning of the experiment there were mild temperatures and even above zero for a short period. Between first and second cooling events there was a period when the air temperature was above zero more than one day. Temperature profile through the rubble responded to the cooling events accordingly with almost no delay and caused propagation of cold front down inside the rubble (Figure 2b). In the beginning there was no snow insulation and temperature of the top surface of the rubble keel followed air temperature, while after March 7th snow came and total effective atmospheric cooling at the keel top surface during 14 days was considerably lower: FDD_{ice} = 42 °C days against FDD_{air} = 104 °C days in the air (Figure 2a). Vertical heat flux due to conduction in the rubble varied from 20 to 80 Wm^{-2} during first two cooling events and exceeded 120 Wm^{-2} during the third one (Figure 2c).

Both conductivity sensors placed inside the rubble showed lower salinity, in the beginning, compare to the salinity of surrounding waters (Figure 3a). Readings at CTS1 and CTS3 began at the levels of about 26 and 29 gkg^{-1} respectively and gradually increased. In the case of CTS1, it reached about 31 gkg^{-1} and rapidly dropped to 0, where stayed until the end of the experiment. This moment was interpreted as a freezing event – CTS1 event (Figure 3a). In the case of CTS2 absolute salinity in the cavity was growing until it established finally at the level of 33.4 gkg^{-1}, where it stayed until the end of the experiment. The rapid increase of the absolute salinity, prior it established at the final level, was interpreted as penetration of the surrounding water inside the cavity – CTS2 event. The absolute salinity of seawater measured below the rubble and level sea ice varied at the level 33.7 gkg^{-1} through the experiment. Based on registered absolute salinity freezing point temperature of water at different points (CTS1, CTS2, CTS3) was calculated and compared with registered temperatures in those points respectively (Figure 3b, c, d). Inside the rubble (CTS1 and CTS2) the registered temperature of the water was below the freezing point temperature, while below the rubble (CTS3) registered temperature of water was below its freezing point temperature. In the upper part of the rubble (CTS1) (Figure 3a) difference between freezing temperature and registered temperature was about 0.3 °C in the beginning and then freezing temperature was decreasing, and the difference became 0.15 °C at the moment of the CTS1 freezing event. In the bottom part of the rubble difference between freezing temperature and the registered temperature began with up to 0.5 °C and reduced to less than 0.1 °C due to a decrease of freezing temperature. Sea water temperature below the rubble (CTS3) was above freezing point temperature all time during the experiment (Figure 3d). The difference between registered temperature and freezing temperature was growing during the experiment from the initial value of 0.15 °C to final 0.2 °C. Freezing point temperature was varied with salinity fluctuations in the range between -1.85 to -1.84 °C with a noticeable increase towards the end of the observation period.

Comparison of temperature and salinity profiles in level ice before and in rubble field after the experiment is shown in Figure 4. Ice cores were taken respectively in the level ice and rubble field. Before coring samples, ice rubble was lifted up, and the consolidated layer of up to 30 cm thickness was observed (Figure 5). For the level ice temperature profile was measured in situ, while for the rubble field, readings from thermistor string probe are shown inside the keel part. Salinity profiles were constructed by melting respective sections of the ice cores in both cases.

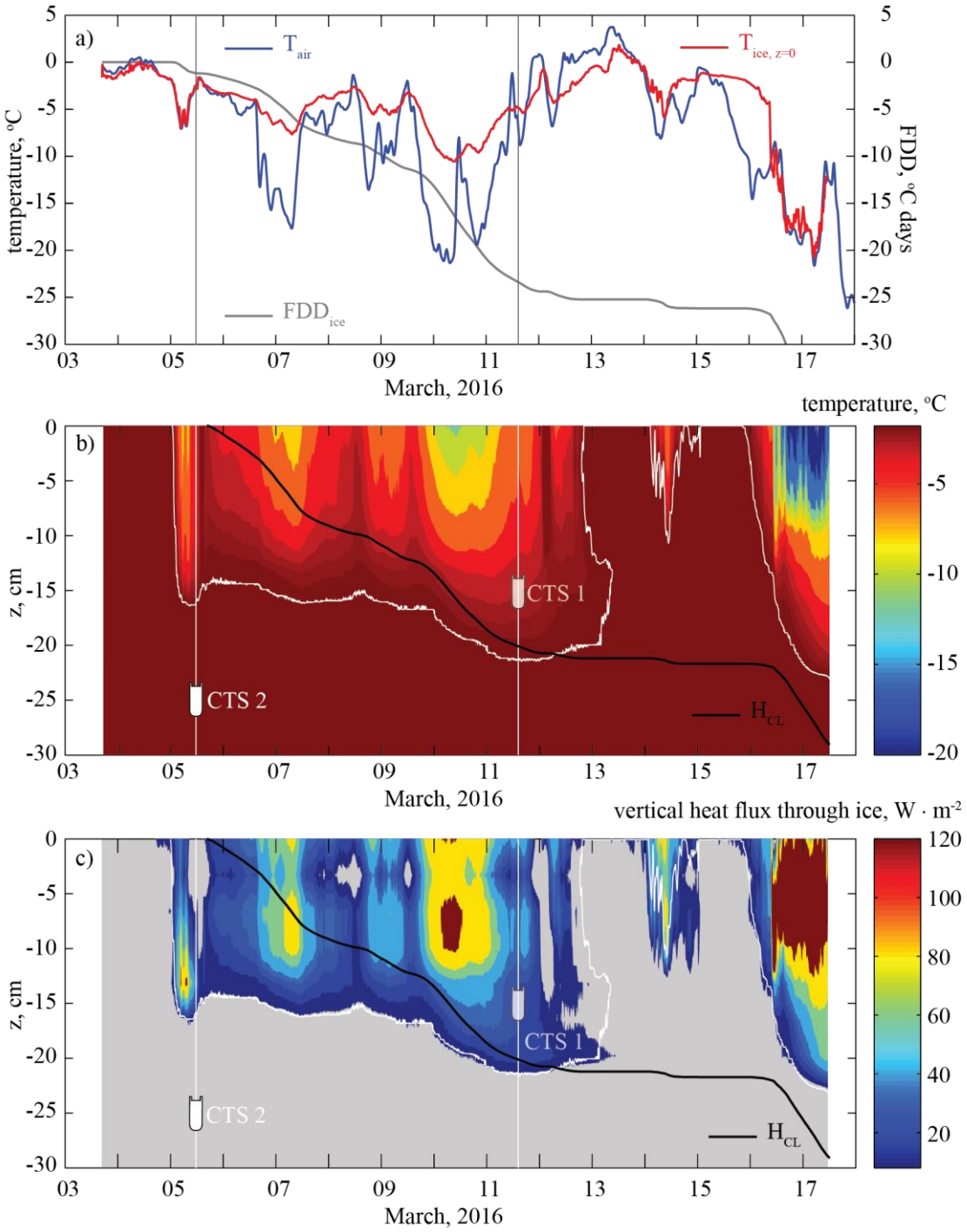

Figure 2. Air temperature close to the ice surface, ice temperature and freezing degree days at the top surface of the keel (a). The temperature profile of ice rubble measured by thermistor string and plotted in time-height space (white line shows isotherm T=-1.8 °C) (b). Vertical heat flux through the rubble, calculated using thermistor string data according to Fourier's law (c) (thermal conductivity 2.1 $Wm^{-1}K^{-1}$, temperature gradient is calculated correspondingly between each two following temperature measuring points). Black curves show consolidated layer thickness of ice rubble calculated using Stefan's equation. Vertical lines on all plots and white signs of CTS sensors are related to the time moments of two respective events happened at two different CTS sensors. Note that positions of CTS sensors are rather qualitative while time moments logged in data series.

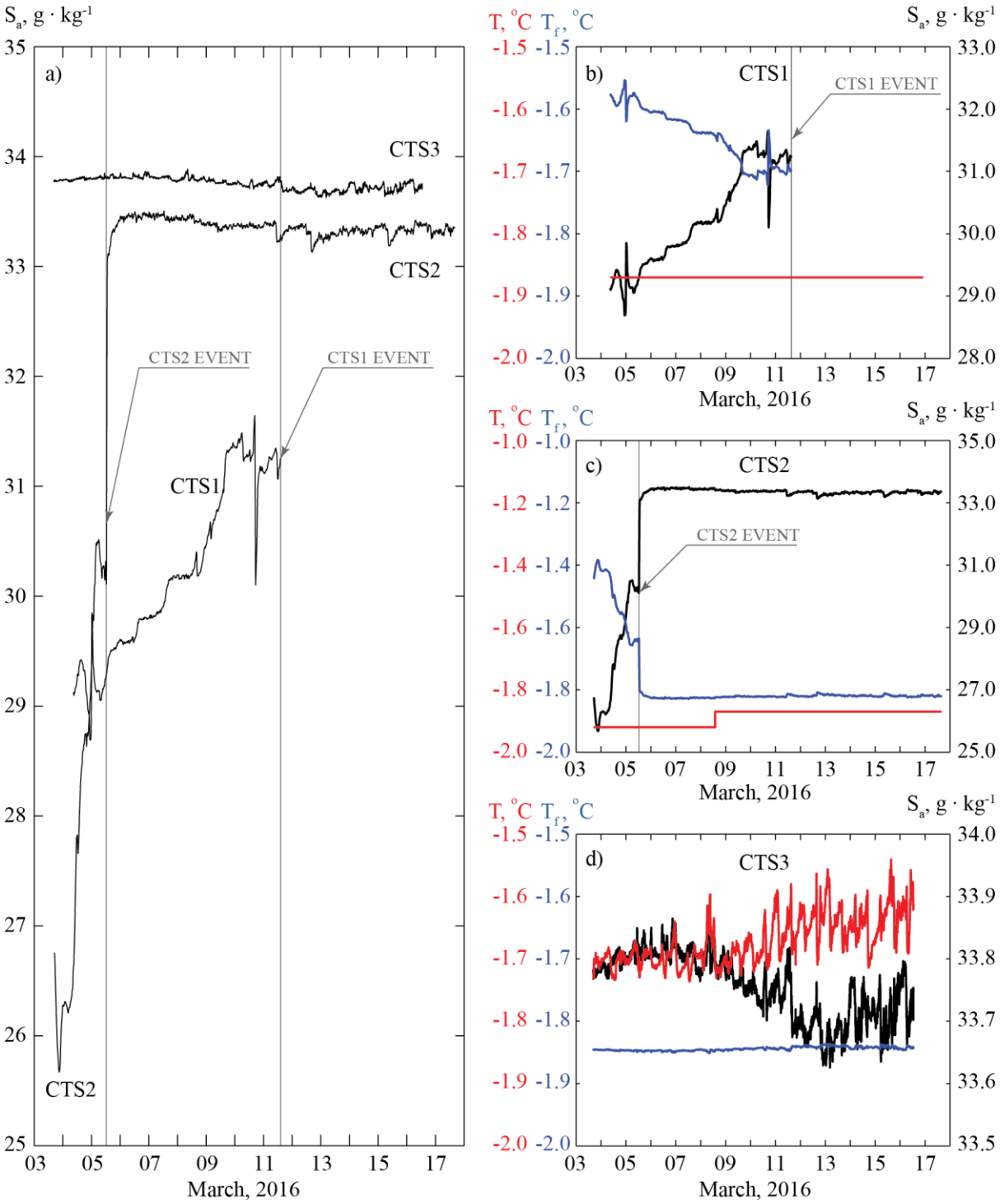

Figure 3. The absolute salinity of water measured in all three points: CTS1, CTS2, and CTS3 respectively (a). Actual temperature, absolute salinity and calculated freezing point temperature for CTS1, CTS2 and CTS3 in (b), (c) and (d).

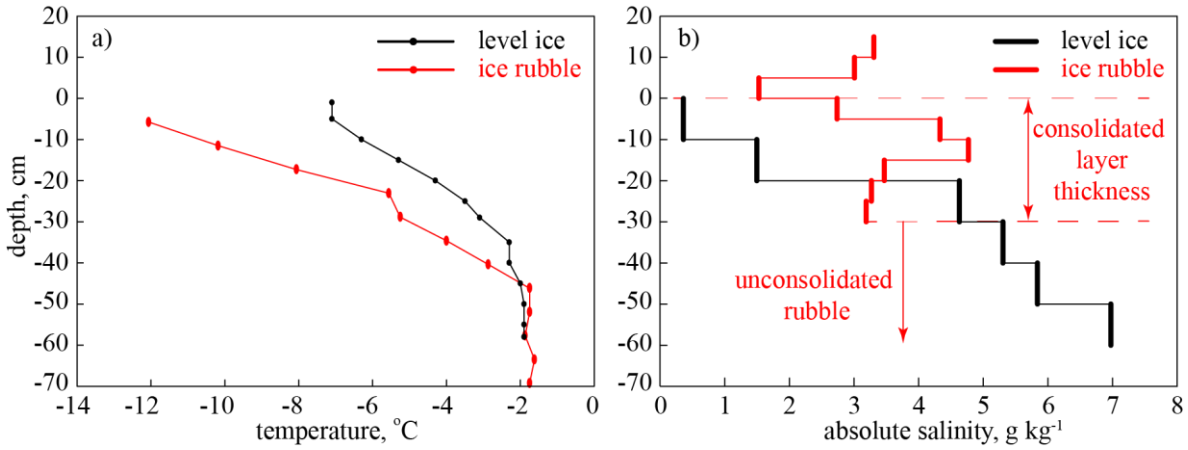

Figure 4. Temperature (a) and salinity (b) profiles in the level ice at the beginning of the experiment (black curves) and in the rubble field (red lines) at the end of the experiment.

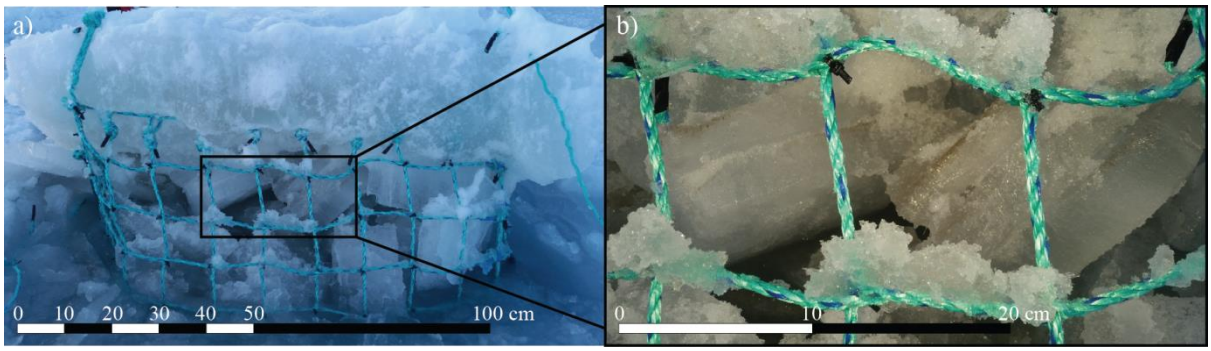

Figure 5. Consolidated layer of rubble and unconsolidated rubble below it at the end of experiment (a); zoomed view of the bottom part of the consolidated layer, where single blocks are frozen, while cavities between them are not (b).

DISCUSSIONS

Estimated ice rubble consolidated layer thickness calculated from Stefan's equation (Stefan, 1891) using temperature at the top surface of the keel predicts the final thickness of consolidated layer defined by the thermal isoline or zero temperature gradient line (Figure 2b, c). Note that increase in temperature of ice rubble during June 13th – 16th (Figure 2b) does not cause its melting. Sea ice can be heated above freezing point temperature of saline water from which it was formed; any change in temperature of saline ice causes the adjustment of brine volume fraction on the micro-porosity scale. During mentioned period of no atmospheric cooling, the thickness of consolidated layer has to be considered kept at the same level until the new event of atmospheric cooling will occur. The difference (Figure 2b, c) in consolidated layer thickness between one defined by the isothermal line (and zero temperature gradient line) and one calculated using Stefan's equation can be caused by reserved cold and process during the initial phase of consolidation; and also by affected temperature measurements. The used thermistor string probe consists of sensors placed into the metal tube and filled with some thermal isolation material between sensors. Metal coater has a higher thermal conductivity compare to ice, what cause cold to propagate locally down into rubble along the probe (see the beginning of the cooling events on 5th, 14th and 16th of June, Figure 2b). One can see that cold temperature front first rapidly penetrates down and then in several hours it lifts back up again. In particular, such strikes are the consequence of the warm temperatures in general and probe not being frozen properly (not in full contact)

into ice. This is short time phenomena, but on the long run, it is not excluded that conduction along the probe affects results noticeably. That has to be studied.

As shown in results (Figure 3a), CTS1 and CTS2 inside the rubble experienced lower salinity, in the beginning, compare to a salinity of surrounding water measured by CTS3. This must be due to the melting of ice blocks to provide the source of the fresher water. However, what was the exact reason of melting is remaining an open question. Surrounding water was above the freezing point temperature (Figure 3d). Thus we can expect considerable oceanic heat flux towards the rubble from below. The fact that salinity in the cavity of CTS2 (deeper in rubble) lower than in cavity with CTS1 (higher in rubble), is for the hypothesis that melting is caused by the high oceanic turbulent heat flux. Since the lower part of the rubble exposed more to the oceanic flux, there is more melting occurs and lower salinity drops. Further, in the experiment, both sensors CTS1 and CTS2 showed an increase of water salinity in cavities where sensors were measuring. There were two events noticed related to salinity change: CTS1 event and CTS2 event. First, in time, CTS2 event occurred when salinity in cavity rapidly jumped to the value close to surrounding water salinity (CTS3) and further stayed at that level (Figure 3a, c). In total salinity has grown from 25.7 to 33.5 g kg^{-1} during two days. As we think, while melting of the rubble from below was developing, at the same time it was increasing permeability of the upper rubble to the sea water. At the moment when cavity with sensor became accessible to sea water, salinity in the cavity instantly jumped (CTS2 event). Second, in time, the CTS1 event occurred, when, as we believe, conductivity measuring cell got frozen and as a result salinity readings instantly dropped to zero. Whether only measurement cell or the entire cavity got frozen is an open question. In the case of CTS1, the rate of salinity increase was lower, during six days salinity has grown from 29 to 31 g kg^{-1} (Figure 3a, b). Temperature readings of CTS1 and CTS2 show that both cavities were supercooled (Figure 3b, c) with temperatures close to the freezing point temperature of sea water (Figure 3b, c, d). In the case of CTS1 water in the cavity was supercooled up to 0.3 °C in the beginning, while conductivity measurement cell got frozen when water was supercooled by 0.2 °C. Since we do not observe temperature decrease in CTS1 data (Figure 3b) after conductivity measurement cell got frozen, the conclusion pending to be that only measuring cell got frozen, while the cavity remained unfrozen. Otherwise, we would observe temperature drop, due to cold temperature front propagation down once ice cavity is frozen. The facts that we cannot see a drop in the temperature at CTS1 and that its value is higher compared to the thermistor probe temperature value at the same level, are consistent with the suggestion made above that metal coating of the thermistor probe can affect the measurements and bring to the observed situation. One should understand that larger spacing between sensors in thermistor string probe makes results very discrete and hard to observe thermal processes with high spatial resolution, while CTS1 and CTS2 measure directly inside the cavities between ice blocks.

Due to a different sequence of submerging blocks and their orientation in the rubble field, we cannot expect similarity in salinity profiles between level ice and ice rubble. At the end of the experiment salinity profile in the rubble varies between 2 and 5 g kg-1 compare to 0 and 7 g kg-1 for level ice respectively (Figure 4b). Since the upper bound of the range is becoming less, there are no new salt sources in the ice rubble, i.e. cavities between ice blocks have possibilities to expel salts out below it while freezing. This probably can explain a maximum of salinity in ice rubble at the level of 10-20 cm depth.

At the end of the experiment keel of the rubble field consisted of three parts: a) fully consolidated layer with frozen cavities; b) consolidated layer part where ice blocks frozen together while cavities were not frozen and c) unconsolidated loose ice blocks (Figure 5).

CONCLUSIONS

The small-scale field experiment on ice rubble thermodynamic consolidation was conducted in Van Mijen Fiord, Spitsbergen in March 2016. One of the most important aspects of studies was put on the processes related to salt balance inside the cavities between ice blocks. In conditions of mild atmospheric cooling (FDD_{air} = 104 °C days, which with snow and sail insulation resulted in FDD_{ice} = 42 °C days) and sea water being above freezing temperature by up to 0.2 °C, at the end of the experiment (after 14 days) we observed a consolidated layer up to 30 cm thick.

Water inside both cavities between ice blocks at two different levels was all time supercooled by up to 0.3 °C. It was indicated that oceanic heat flux continuously melts bottom part of the unconsolidated part of the keel; what results in two processes: it provides fresher water and at the same time makes the bottom part of the keel more permeable to the seawater of high salinity. At the same time ice cavities in the upper layers of the rubble, which are subjected to freezing, have possibilities to expel salt further below them as they freeze.

Temperature data interpretation using thermal isoline (or zero temperature gradient isoline corresponding to the sea water freezing temperature gives a reasonable estimate of the final thickness of consolidated layer compared to the thickness calculated according to Stefan's equation using FDD_{ice} = 42 °C days (Figure 2). At the same time, it was seen that metal coating of the thermistor string probe should preferably be avoided to reduce the thermal conductivity of the probe itself. Moreover, at the scale experiment was performed, higher spatial resolution of thermistor string would be beneficial to catch more local processes in the cavities.

At the end of the experiment all three expected parts of rubble keel were observed: a) fully consolidated layer with frozen cavities; b) consolidated layer part where ice blocks are frozen together while cavities were not frozen and c) unconsolidated loose ice blocks (Figure 5). Consolidated layer thickness as defined by isoline corresponding to sea water freezing temperature and zero temperature gradient, by mechanical drilling and by Stefan's equation is 23, 30 and 29 cm correspondingly.

ACKNOWLEDGEMENTS

The author wishes to acknowledge the support of the Research Council of Norway through the Centre for Research-based Innovation SAMCoT (project number 203471) and the support of all SAMCoT partners.

REFERENCES

Blanchet, D., 1998. Ice loads from first-year ice ridges and rubble fields. Canadian Journal of Civil Engineering, 25(2): 206-219.

CAN/CSA-S471-92, R2001. General Requirements, Design Criteria, the Environment, and Loads. Standards Council of Canada.

GeoPrecision, 2017. Environmental Technology for Industry, Science and Research (http://www.geoprecision.com/en/).

Hansen, E., Gerland, S., Granskog, M.A., Pavlova, O., Renner, A.H.H., Haapala, J., Løyning, T.B. and Tschudi, M., 2013. Thinning of Arctic sea ice observed in Fram Strait: 1990–2011. Journal of Geophysical Research: Oceans, 118(10): 5202-5221.

Høyland, K.V., 2002. Consolidation of first-year sea ice ridges. Journal of Geophysical Research: Oceans, 107(C6): 15-1-15-16.
IOC, SCOR and IAPSO, 2010. The international thermodynamic equation of seawater – 2010: Calculation and use of thermodynamic properties. Intergovernmental Oceanographic Commission, Manuals and Guides, UNESCO (English), 56(56): 196.
ISO/FDIS/19906, 2010. Petroleum and natural gas industries - Arctic offshore structures. International Standarization orginaization, Geneva, Switzerland.
Leppäranta, M., Lensu, M., Kosloff, P. and Veitch, B., 1995. The life story of a first-year sea ice ridge. Cold Regions Science and Technology, 23(3): 279-290.
McDougall, T.J., Jackett, D.R., Millero, F.J., Pawlowicz, R. and Barker, P.M., 2012. A global algorithm for estimating Absolute Salinity. Ocean Sci., 8(6): 1123-1134.
Renner, A.H.H., Gerland, S., Haas, C., Spreen, G., Beckers, J.F., Hansen, E., Nicolaus, M. and Goodwin, H., 2014. Evidence of Arctic sea ice thinning from direct observations. Geophysical Research Letters, 41(14): 5029-5036.
Schwerdtfeger, P., 1963. The thermal properties of sea ice. Journal of Glaciology, 4: 789-807.
Shestov, A. and Ervik, Å., 2016. Studies of Drifting Ice Ridges in the Arctic Ocean during May-June 2015. Part II. Thermodynamic properties and melting rate, Proceedings of 23rd IAHR International Symposium on ICE 2016, Ann Arbor, Michigan, USA.
Shestov, A., Hoyland, K.V. and Ervik, Å., 2017. Thermodynamics of Ice Ridges during Spring Season in the Arctic Ocean. Journal of Geophysical Research: Oceans (submitted).
Shestov, A.S. and Marchenko, A.V., 2016a. The consolidation of saline ice blocks in water of varying freezing points: Laboratory experiments and computer simulations. Cold Regions Science and Technology, 122: 71-79.
Shestov, A.S. and Marchenko, A.V., 2016b. Thermodynamic consolidation of ice ridge keels in water at varying freezing points. Cold Regions Science and Technology, 121: 1-10.
SNiP2.01.07-85, 1987. Construction Codes and Regulations. Loads and Forces. Techincal Standards Used in Russia and Kazakhstan, pp. 34.
Spreen, G., Kwok, R. and Menemenlis, D., 2011. Trends in Arctic sea ice drift and role of wind forcing: 1992–2009. Geophysical Research Letters, 38(19): n/a-n/a.
Star-Oddi, 2017. Fish tagging & data logging with data storage tags (http://www.star-oddi.com/).
Stefan, J., 1891. Theory of ice formation, especially in the Arctic Ocean (German). Ann. Physik, N.f: 269-286.
Strub-Klein, L. and Høyland, K.V., 2011. One Season of a 1st Year Sea Ice Ridge Investigation - Winter 2009, Proceedings of 21th International Conference on Port and Ocean under Arctic Conditions (POAC) Montreal, Canada.
Strub-Klein, L. and Sudom, D., 2012. A comprehensive analysis of the morphology of first-year sea ice ridges. Cold Regions Science and Technology, 82(0): 94-109.
Timco, G.W. and Burden, R.P., 1997. An analysis of the shapes of sea ice ridges. Cold Regions Science and Technology, 25(1): 65-77.